

FULL PAPER

Open Access



Time variations in the chemical and isotopic composition of fumarolic gases at Hakone volcano, Honshu Island, Japan, over the earthquake swarm and eruption in 2015, interpreted by magma sealing model

Takeshi Ohba^{1*}, Muga Yaguchi², Kana Nishino¹, Nozomi Numanami¹, Yasushi Daita³, Chiho Sukigara^{4,5}, Masanori Ito⁴ and Urumu Tsunogai⁴

Abstract

Definite increases in the components ratios of $\text{CO}_2/\text{H}_2\text{O}$, $\text{CO}_2/\text{H}_2\text{S}$, CO_2/CH_4 and He/CH_4 were observed at the fumarolic gases from Owakudani geothermal area located at the center of Hakone volcanic caldera (Honshu Island, Japan), synchronized with the earthquake swarm in 2015. Such variations were due to the dominance of a magmatic component over a hydrothermal component, suggesting the earthquake swarm was produced by the injection of magmatic gases into the hydrothermal system. The $\text{CO}_2/\text{H}_2\text{O}$ ratio of magmatic gas was estimated to be 0.0045 before the earthquake swarm, which increased up to 0.013 during the earthquake swarm, likely produced by the pressurization of magma as a result of magma sealing where the pressure increment in magma was estimated to be 3% to the lithostatic pressure. The H_2O and CO_2 concentration in magma were estimated to be 6.3 wt% and 20 wt ppm, respectively, assuming a temperature 900 °C and a rhyolitic composition. In May 2015, a few months prior to the earthquake swarm in May 2015, a sharp increase in the Ar/CO_2 and N_2/He ratios and a decrease in the isotopic ratio of H_2O were observed at the fumarolic gas. The invasion of air into the hydrothermal system increased the Ar/CO_2 and N_2/He ratios. The decrease in the isotopic ratio of H_2O was induced by partial condensation of H_2O vapor.

Keywords: Active volcano, Fumarolic gas, Earthquake swarm, Phreatic eruption, Mt. Hakone, Magma degassing, Magma sealing

Introduction

Mt. Hakone is an active volcano located on Honshu Island of Japan (Fig. 1a). The volcano has a caldera structure with several central cones (Fig. 1b). Three geothermal areas: Owakudani (Ow in Fig. 1c), Kamiyuba (Ky) and Sounzan (So) developed as the foothill of Kamiyama (Ka) central cone. The history of caldera formation was first proposed by Kuno (1950) and modified by Manen (2008). The geothermal area of Ow is a popular

sightseeing spot visited by two million tourists every year. In order to prevent human injury by possible eruption, a monitor program was started in the 1970s at Mt. Hakone.

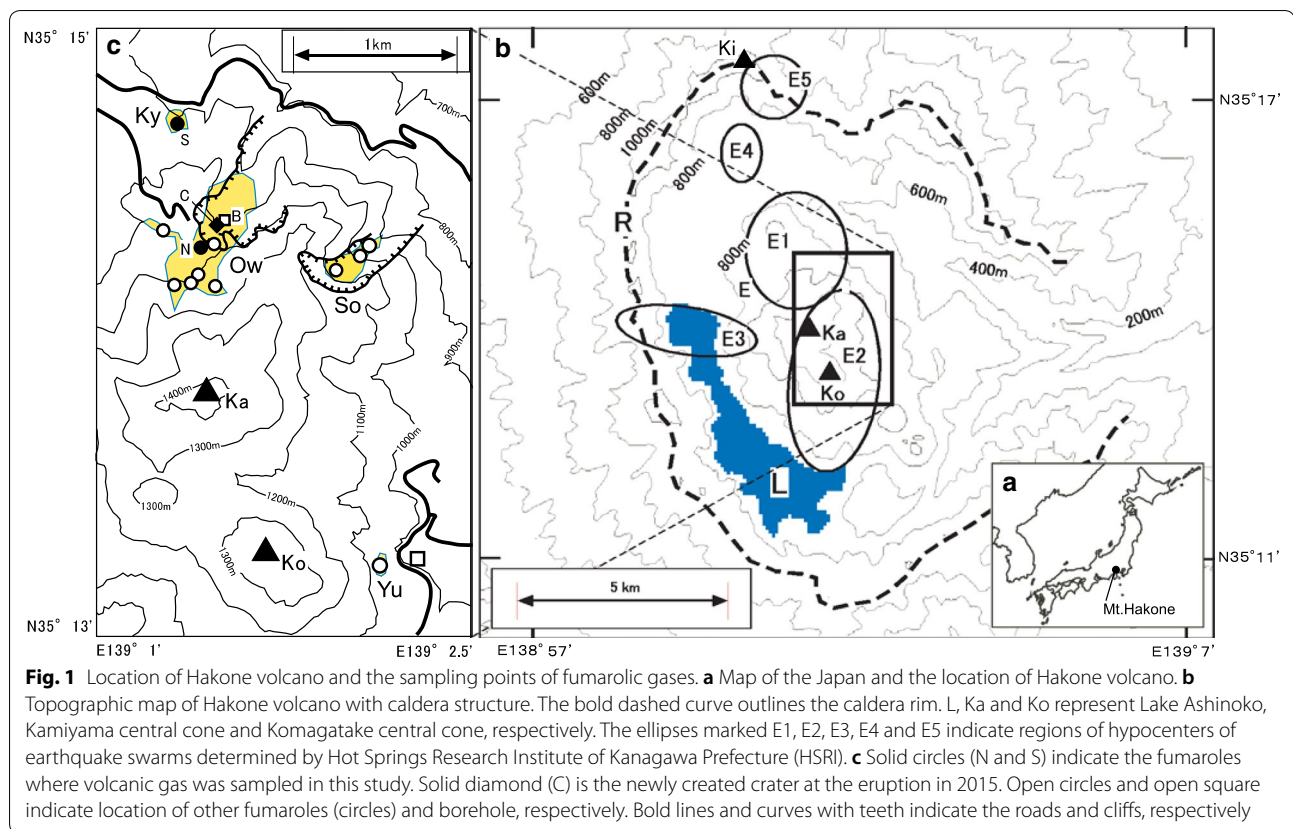
Eruptive activity at the central cones took place 50 ka ago and continued until 3 ka ago (Kobayashi et al. 1997), when a phreatic eruption occurred. With the phreatic eruption, a section of the western flank of Ka (Fig. 1c) collapsed and caused debris flow, damming a river to form Lake Ashinoko in Fig. 1b. No historical eruption has been recorded at Hakone volcano before the small phreatic eruption in 2015 at the geothermal area of Ow.

Based on the analysis of seismic wave velocities beneath Hakone caldera, Yukutake et al. (2015) recognized a

*Correspondence: takeshi_ohba@tokai-u.jp

¹ Tokai University, 4-1-1 Kitakaneme, Hiratsuka, Kanagawa 259-1291, Japan

Full list of author information is available at the end of the article



region with high V_p/V_s ratio beneath Ko (Fig. 1c) likely due to a degassing magma as the depth of ~ 10 km. Above the degassing magma, a region with low V_p/V_s ratio was found, which was estimated to be a gas reservoir dominated by H_2O and CO_2 . In 2001 to 2009, volcanic gases and borehole gases were analyzed by Ohba et al. (2011). The CO_2/H_2O and CO_2/H_2S ratios were high in 2001 when a seismic swarm occurred. It increased again in 2006 and 2008 when a new seismic swarm resumed. The increases in CO_2/H_2O and CO_2/H_2S ratios suggested the injection of a CO_2 -rich magmatic gas into the hydrothermal system, implying that a magmatic component was episodically supplied to the hydrothermal system in 2006 and 2008. The earthquake swarms resulted from the injection of the gas through the shallow crust accompanying the break of the so-called sealing zone (Fournier 1999). Daita (2013) monitored fumarole S (Fig. 1c) at Ky geothermal area in 2012 and 2013 by using a gas detector tubes system (GASTEC corp.), when a sharp increase in CO_2/H_2S ratio, synchronized with the start of seismic swarm, was found.

At Hakone volcano, an earthquake swarm started on April, 26, 2015. On June, 30, 2015, a small phreatic eruption occurred at the geothermal area of Ow. After the eruption, several craters formed (Mannen et al. 2018).

The C crater in Fig. 1c is one of the newly born craters. In this study, we repeatedly sampled fumarolic gas at Ow and Ky geothermal areas for investigating the relationship between volcanic activity and volcanic gas chemistry.

Sampling and analysis of fumarolic gases

Fumarolic gases were sampled every month from May 2013 until February 2018, at the points N and S (Fig. 1c). In addition, fumarolic gases were sampled at point C (Fig. 1c). The outlet temperature of fumarolic gas was measured by a thermocouple with K-type sensor. Gas sampling was carried out by a titanium pipe inserted into the fumarole which was then connected to a rubber tube. The rubber tube was connected to a 120-ml pre-evacuated Pyrex glass bottle with airtight stop cock (Giggenbach 1975), where 20 ml of 5 M KOH solution was added. Steam-condensated and acidic gases (CO_2 , SO_2 , H_2S , HCl etc.) were absorbed by the KOH solution, whereas the residual gases (hereafter R-gas), e.g., N_2 , O_2 , Ar, He, H_2 and CH_4 , enriched in the headspace of glass bottle. Components in the KOH solution were analyzed according to the method by Ozawa (1968). The SO_2/H_2S ratio in the fumarolic gas was determined using a KI-KIO₃ solution (Ozawa, 1968), the analytical accuracy of which was evaluated

by Lee et al. (2016). The analysis of HCl was only carried out at the fumarole C. The total molar amount of R-gas was given by the head space volume of bottle and the inner pressure of head space as room temperature. Based on the molar amount of H₂O, CO₂, H₂S, SO₂ and R-gas, the relative concentration (μmol/mol) of those components was calculated (Tables 1, 2 and 3).

The R-gas was analyzed by using two different gas chromatographs with Ar and He as gas carriers (hereafter GC-Ar and GC-He, respectively). Concentration of He, H₂, O₂, N₂ and CH₄ was determined by GC-Ar equipped with a 6 m-long MS5A packed column and a TCD detector. The temperature of the column and detector was kept at 50 and 100 °C during analysis, respectively. The flow rate of Ar was 30 ml/min. In general, He analysis by GC is difficult due to the overlap where H₂ has high concentrations. Under the above condition, the He of 64 ppm in R-gas could be separated from the H₂ of 67% in R-gas without the overlap between the chromatographic peaks of He and H₂. All of R-gas sample in this study had a good separation between He and H₂ peaks.

The relative concentration of N₂ and Ar was determined by GC-He. In the GC-He, equipped with a 6 m-long Gaskuropack-54 column (GC Sciences Inc.) and a TCD detector, the temperature of the column and detector was kept at −70 and 50 °C, respectively. Under the above conditions, N₂, O₂ and Ar in R-gas were well separated on the chromatographic chart. The concentration of Ar in R-gas was calculated by,

$$X_{\text{Ar}} = X_{\text{N}_2} \frac{R_{\text{Ar}}}{R_{\text{N}_2}}, \quad (1)$$

where X and R indicate the concentration obtained by GC-Ar and GC-He, respectively.

The H₂O isotopic ratio was determined by the cooling of the fumarolic gas with a double tube condenser made of Pyrex glass. The fumarolic gas flowing out of the condenser was collected in a 5-l plastic gas sampling bag. The gas collected in the bag was used for on-site determination of CO₂/H₂S molar ratios by gas detector tube system. We used “2HH” and “4HH” detector tubes for the measurement of CO₂ and H₂S, respectively. The applicable range of concentration for 2HH and 4HH was 5–40% and 0.1–2.0%, respectively.

The isotopic ratio of condensed water was determined by an IR-laser cavity ring-down analyzer (Picarro Inc., L2120-i). The analytical precision of the analyzer was ±0.12 and ±0.05‰ for δD and δ¹⁸O, respectively. The isotopic ratio of H₂ in R-gas was determined by a continuous flow system combined with a mass spectrometer (Thermo Fisher Scientific Delta V) (Tsunogai et al. 2011). The analytical precision of the analyzer was ±0.8‰ for δD.

Results

The analytical results of fumarolic gases at N, S and C are listed in Tables 1, 2 and 3, respectively. Time variations of CO₂/H₂O, H₂S/H₂O, CO₂/H₂S, CO₂/CH₄ and He/CH₄ ratios are shown in Fig. 2 with the number of earthquakes per half month at Hakone volcano observed by Japan Meteorological Agency (JMA). On April, 26, 2015, the earthquake swarm started (Mannen et al. 2018). The hypocenters of earthquakes were distributed in the regions E1 to E4 of Fig. 1b (Mannen et al. 2018). The magnitude of earthquakes during the unrest was <2.9. The largest earthquake was observed on the July, 21, 2015 (Mannen et al. 2018). On the May, 15, 2015, the largest daily number of earthquake (955, $M \geq 0$) was observed (Mannen et al. 2018). In the E5 region of Fig. 1b, a small earthquakes swarm took place in 2017 in which the largest earthquake ($M=1.5$) occurred on the April 11 (<https://www.onken.odawara.kanagawa.jp/earthquake/>).

In May 2015, the CO₂/H₂O ratio increased up along with the frequency of earthquakes (Fig. 2a), and then, the earthquake events decreased after May 2015, as well as the CO₂/H₂O ratio. Similar increases and decreases were observed in the ratios CO₂/H₂S, CO₂/CH₄ and He/CH₄ along the occurrence of earthquakes in 2015 (Fig. 2c, d, 2, respectively). For the indication in Fig. 2c, the CO₂/H₂S ratio determined by gas detector tubes system was used. The corresponding CO₂/H₂S curve determined by chemical analysis was not smooth compared with the curve in Fig. 2c, likely due to the contamination of native sulfur particles during the sampling. There was abundant native sulfur sublimate around the fumarole outlet, because the insertion of a titanium tube during sampling likely disturbed the fumarolic gas discharge, releasing particles of native sulfur. The native sulfur contamination increases the amount of sulfur dissolved in KOH solution.

The gradual decrease in the CO₂/H₂S, CO₂/CH₄ and He/CH₄ ratios after the maximum in 2015 continued until around March 2017, followed by a gradual increase which peaked in September 2017. The increase in 2017 was not clear in CO₂/H₂O ratio due to the fluctuation (Fig. 2a). No increase was observed in the H₂S/H₂O ratio in May 2015 when the earthquake swarm observed (Fig. 2b). Beside small fluctuations, the H₂S/H₂O ratio was stable over the whole duration of this study.

Time variations of the SO₂/H₂S, H₂/H₂O, Ar/CO₂ and N₂/He ratios are shown in Fig. 3. For the calculation of Ar/CO₂ and N₂/He ratios, the Ar and N₂ brought by the direct contamination of air during sampling were removed by the following equations,

$$C_{\text{Ar}}^* = C_{\text{Ar}} - \left(\frac{0.934}{20.95} \right) C_{\text{O}_2}, \quad (2)$$

Table 1 Chemical and isotopic composition of fumarolic gas sampled at the point N in Owakudani geothermal area, Hakone volcano, Japan

Date yy/mm/dd	Temp °C	*CO ₂ /H ₂ S molar ratio	H ₂ O μmol/ mol	CO ₂ μmol/ mol	H ₂ S μmol/ mol	SO ₂ μmol/ mol	He μmol/ mol	H ₂ μmol/ mol	O ₂ μmol/ mol	N ₂ μmol/ mol	CH ₄ μmol/ mol	Ar μmol/ mol	δD _{SMOW} H ₂ O	δ ¹⁸ O _{SMOW} H ₂ O	δD _{SMOW} H ₂	**AET °C
2013/5/7	95.6		974,800	20,600	4020	92.7	0.0678	209	0.00	251	0.668	0.670	-53	-7.7	-579	141
2013/6/4	97.5		981,400	15,160	3040	105	0.0305	158	0.00	173	0.455	1.664	-55	-7.2	-608	115
2013/7/9	96.8		988,200	9360	2190	39.1	0.0316	123	0.00	107	0.377	0.296	-51	-6.8	-619	105
2013/8/28	97.5		989,300	8320	2140	8.2	0.0265	110	0.00	88	0.337	0.291	-47	-5.7	-618	105
2013/10/2	97.0		986,400	9000	3660	44.8	0.0581	46	0.00	840	0.681	14.3	-58	-7.0	-626	102
2013/11/29	96.6		987,900	8610	3170	29.3	0.0285	101	0.31	236	0.576	2.06	-62	-8.7	-619	109
2014/1/28	96.8		988,400	8610	2790	75.9	0.0260	81	0.41	85	0.461	0.169	-54	-6.6	-625	101
2014/4/25	96.9		992,900	5160	1810	24.4	0.0104	61	1.20	50	0.222	0.252	-45	-5.3	-620	102
2014/5/30	98.7		991,500	6160	2120	36.8	0.0164	101	0.00	78	0.548	0.355	-43	-4.7	-622	100
2014/7/4	97.2		991,800	6140	1940	37.1	0.0190	43	0.31	76	0.388	0.347	-50	-5.9	-626	99
2014/8/6	96.3		991,200	6480	2170	25.3	0.0263	45	0.00	89	0.488	0.452	-50	-5.7	-615	108
2014/9/12	96.8		990,300	7140	2350	73.7	0.0309	60	0.47	106	0.591	0.488	-50	-6.1	-627	98
2014/10/15	96.8	3.5	988,600	8910	2260	76.7	0.0320	70	0.44	116	0.641	0.600	-55	-7.0	-662	72
2014/11/19	97.1	3.3	991,500	6420	1920	33.6	0.0169	31	0.50	64	0.376	0.289	-50	-6.0	-654	77
2014/12/19	96.8	3.4	991,800	6110	1960	18.2							-51	-6.3	-675	61
2015/1/20	97	3.2	992,000	5820	1950	27.9	0.0151	31	18.82	126	0.364	1.03	-51	-6.4	-625	100
2015/2/16	96.5	3.1	990,800	6380	2370	40.4	0.0217	19	0.12	384	0.537	5.86	-57	-7.4	-595	128
2015/3/31	97.2	3.4	989,700	5940	2260	44.0	0.0294	19	249	1750	0.522	29.9	-60	-8.4	-602	123
2015/4/24	95.9	3.6	984,400	6640	3550	34.9	0.0591	36	3.76	5240	0.408	90.4	-67	-10.2	-581	144
2015/5/8	95.6	4.4	988,700	8670	2400	29.0	0.0365	24	0.00	133	0.373	0.364	-56	-7.2	-600	123
2015/6/2	96.1	9.8	979,300	18,250	2150	68.1	0.0718	26	0.09	230	0.276	0.477	-52	-6.7	-607	116
2015/6/16	96.8	9.0	976,000	21,180	2560	30.5	0.0777	30	0.18	244	0.306	0.547	-52	-6.8	-589	131
2015/7/14	96.6	6.8	971,600	24,110	3950	70.0	0.0816	49	0.19	247	0.313	0.647	-51	-6.7	-611	112
2015/7/28	96.3	5.8	979,300	16,980	3480	37.8	0.0657	45	0.05	199	0.255	0.402	-55	-7.4	-613	112
2015/8/20	96.1	4.6	977,200	18,160	4360	33.2	0.0633	46	0.05	204	0.312	0.441	-55	-7.2	-605	118
2015/9/11	96.1	4.4	983,400	13,000	3420	32.7	0.0444	47	0.08	146	0.272	0.316	-56	-7.6	-576	144
2015/10/6	97.2	4.3	984,300	11,990	3490	34.4	0.0360	35	0.05	130	0.257	0.406	-55	-7.3	-608	116
2015/11/11	96.9	4.1	990,100	6590	3150	20.3	0.0307	33	0.07	106	0.252	0.348	-54	-7.1	-602	120
2015/12/8	96.7	4.3	985,300	11,300	3160	29.8	0.0420	54	2.94	187	0.503	1.378	-58	-8.2	-609	116
2016/1/8	96	3.3	983,000	12,580	4190	27.6	0.0339	48	1.51	198	0.517	0.997	-52	-6.5	-579	140
2016/1/28	97.7	3.7	988,400	8290	3160	20.8	0.0260	32	0.36	99	0.367	0.364	-66	-8.9	-612	116
2016/2/15	96.5	3.9	982,200	13,850	3810	16.7	0.0254	40	0.08	105	0.399	0.317	-63	-8.0	-616	112
2016/3/2	96.5	3.8	986,800	9540	3470	36.5	0.0252	35	0.20	113	0.346	0.709	-62	-8.1	-617	110
2016/4/8	96.5	3.2	989,000	7780	3050	74.1	0.0227	35	0.09	97	0.419	0.585	-64	-8.8	-613	114

Table 1 (continued)

Date yy/mm/dd	Temp °C	*CO ₂ /H ₂ S molar ratio	H ₂ O μmol/ mol	CO ₂ μmol/ mol	H ₂ S μmol/ mol	SO ₂ μmol/ mol	He μmol/ mol	H ₂ μmol/ mol	O ₂ μmol/ mol	N ₂ μmol/ mol	CH ₄ μmol/ mol	Ar μmol/ mol	δD _{SNOW} H ₂ O	δ ¹⁸ O _{SNOW} H ₂ O	δD _{SNOW} H ₂	**AET °C
2016/5/13	96.5	3.3	988,900	7520	3280	29.4	0.0173	30	0.15	276	0.394	4.213	-65	-8.1	-619	110
2016/6/3	96.7	3.3	990,900	6190	2710	19.9	0.0170	26	4.09	127	0.392	1.187	-66	-8.4	-615	114
2016/7/5	97.7	3.1	993,300	3640	2980	15.9	0.0135	25	0.06	78	0.353	0.625	-62	-8.3	-618	109
2016/8/5	96.9	3.7	994,000	3480	2320	29.3	0.0160	25	0.11	108	0.380	0.958	-63	-8.1	-613	114
2016/9/5	97	3.2	991,900	5390	2610	26.4	0.0155	53	0.07	62	0.485	0.283	-61	-8.5	-609	117
2016/10/7	96.9	2.7	990,900	5590	2670	9.5	0.0153	29	1.23	685	0.553	9.71	-68	-9.7	-611	117
2016/10/19	97.2	2.7	992,300	5080	2450	23.9	0.0128	57	0.15	54	0.495	0.236	-57	-7.9	-634	95
2016/11/4	96.9	2.9	993,300	4120	2390	25.7	0.0123	58	0.25	55	0.507	0.229	-56	-7.6	-615	110
2016/12/7	96.4	3.1	987,500	8080	3870	90.2	0.0218	87	3.71	399	0.856	6.15	-64	-9.1	-616	112
2017/1/11	96.3	3.2	992,600	5030	2210	56.9	0.0097	53	0.04	49	0.537	0.221	-59	-8.2	-613	112
2017/2/6	95.9	2.9	991,700	5430	2670	92.9	0.0134	60	0.18	59	0.688	0.259	-58	-7.8	-634	95
2017/3/9	95.7	2.8	993,300	4210	2340	81.7	0.0126	53	0.67	52	0.579	0.256	-55	-7.4	-626	101
2017/4/10	96.2	2.5	993,900	3400	2540	45.8	0.0100	47	0.31	51	0.591	0.268	-59	-8.0	-624	103
2017/5/10	96.3	3.1											-84	-12.4	-617	118
2017/6/10	96.1	3.1	982,400	11,400	5640	267	0.0359	101	0.10	144	1.396	0.749	-63	-8.8	-606	120
2017/7/4	96.4	3.2	991,800	5550	2480	22.3	0.0173	45	0.01	65	0.612	0.240	-56	-7.4	-566	153
2017/8/1	96.5	3.5	991,500	6210	2160	17.6	0.0156	37	0.37	72	0.493	0.248	-54	-7.0	-609	115
2017/9/2	96.9	3.7	990,200	7250	2360	22.6	0.0247	45	0.09	105	0.558	0.368	-57	-7.7	-588	133
2017/10/4	95.7	4.0											-72	-11.0	-535	192
2017/11/7	96.8	3.9	988,900	8190	2660	19.4	0.0258	48	0.05	154	0.715	1.04	-67	-9.5	-581	144
2017/12/5	96.0	3.9	991,000	6430	2380	25.3	0.0199	41	0.29	87	0.656	0.283	-61	-8.5	-609	117
2018/1/9	95.5	3.7											-77	-12.2	-604	127
2018/2/5	97.0	3.9	989,400	7610	2860	3.00	0.0220	70	0.17	89	0.862	0.360	-62	-8.8	-603	122

*Ratio determined by "Gas detector tubes system"

**Apparent equilibrium temperature defined between δD of H₂O and H₂

Table 2 Chemical and isotopic composition of fumarolic gas sampled at the point S in Kamiyuba geothermal area, Hakone volcano, Japan

Date yy/mm/dd	Temp °C	*CO ₂ /H ₂ S Molar ratio	H ₂ O μmol/ mol	CO ₂ μmol/ mol	H ₂ S μmol/ mol	SO ₂ μmol/ mol	He μmol/ mol	H ₂ μmol/ mol	O ₂ μmol/ mol	N ₂ μmol/ mol	CH ₄ μmol/ mol	Ar μmol/ mol	δD _{SMOW} H ₂ O	δ ¹⁸ O _{SMOW} H ₂ O	δD _{SMOW} H ₂	**AET °C
2013/5/7	98.1		978,600	20,200	500	12.2	0.0609	415	0.000	287	1.47	0.735	-52	-6.8	-636	91
2013/6/4	96.5		986,500	12,540	396	7.00	0.0536	343	0.000	235	1.32	0.551	-54	-7.1	-638	90
2013/7/19	97.5		985,400	13,770	381	9.50	0.0392	302	0.000	187	1.23	0.519	-52	-7.4	-637	91
2013/8/28	97.3		983,000	15,940	499	5.90	0.0409	341	0.000	203	1.33	0.701	-47	-5.9	-630	95
2013/10/2	96.5		989,800	9410	365	9.00	0.0276	289	0.000	144	1.06	0.472	-51	-6.2	-636	91
2013/11/29	96.5		991,900	7210	465	0.50	0.0279	252	0.000	142	1.21	0.292	-49	-6.0	-634	93
2014/1/28	96.9		990,600	8300	607	19.3	0.0349	277	0.000	155	1.39	0.363	-50	-5.9	-631	95
2014/4/25	98.2		988,900	10,250	429	19.4	0.0267	286	0.000	153	1.31	0.543	-50	-6.0	-629	96
2014/5/30	97.1		988,700	10,340	473	10.5	0.0279	273	0.000	155	1.21	0.637	-48	-5.8	-631	94
2014/7/4	97.2		989,100	9890	529	6.20	0.0395	273	0.147	150	1.23	0.567	-51	-6.1	-633	93
2014/8/6	97		989,900	9200	430	9.50	0.0263	277	0.122	141	1.34	0.426	-49	-5.9	-627	98
2014/9/12	97.4		988,500	10,430	586	18.4	0.0367	314	0.000	174	1.70	0.534	-50	-6.0	-655	76
2014/10/15	97.1	23	986,900	12,160	484	18.0	0.0466	233	0.141	171	1.66	0.446	-53	-6.7	-666	68
2014/11/19	97	23	988,600	10,210	868	17.6	0.0405	205	0.307	127	1.24	0.403	-49	-5.9	-630	95
2014/12/19	97.2	21	989,300	9850	517	20.9	0.0283	177	0.347	129	1.42	1.05	-49	-6.0	-628	97
2015/1/20	98.6	20	990,100	8960	674	23.8	0.0231	159	0.314	117	1.15	0.338	-48	-5.8	-631	94
2015/2/16	97.3	19	988,600	10,550	517	8.50	0.0413	198	0.000	143	1.56	0.423	-49	-5.8	-624	100
2015/3/31	98.7	19	991,100	8170	398	20.2	0.0315	167	0.000	113	1.28	0.320	-49	-5.7	-611	111
2015/4/24	97.6	20	990,200	8890	577	11.7	0.0381	184	0.146	128	1.32	0.310	-50	-6.2	-609	113
2015/5/8	97.3	31	984,000	14,920	668	15.0	0.0645	183	0.000	238	1.24	0.426	-52	-6.3	-616	108
2015/5/11	97.6	38	981,400	17,600	552	7.80	0.0831	190	0.000	280	1.18	0.466	-54	-6.8	-564	154
2015/5/19	96.6	47	973,300	24,540	1550	40.9	0.106	236	0.625	363	1.21	0.603	-53	-6.5	-589	131
2015/6/2	96.2	54	975,100	23,830	481	14.6	0.0969	227	0.261	323	1.11	0.722	-48	-5.9	-607	114
2015/6/16	97.1	53	975,200	23,820	477	9.20	0.0878	234	0.394	299	1.10	0.493	-49	-6.0	-616	106
2015/6/30	97.8	59	975,300	23,520	605	19.1	0.0835	216	0.000	291	1.13	0.586	-47	-5.5	-606	114
2015/7/14	98.1	48	977,400	21,520	511	3.00	0.0930	280	0.256	295	1.44	0.676	-55	-7.2	-606	117
2015/7/28	97	41	978,600	20,320	611	9.60	0.0663	245	0.033	236	1.35	0.509	-54	-7.1	-595	126
2015/8/20	97.8	37	978,500	20,270	641	22.4	0.0540	300	0.000	255	1.47	0.556	-50	-6.3	-598	123
2015/9/11	96.6	35	981,600	17,400	507	6.70	0.0493	300	0.021	226	1.37	0.542	-51	-6.7	-618	106
2015/10/6	97.6	33	966,200	31,130	1820	38.0	0.0855	422	0.000	406	2.31	1.12	-60	-8.0	-607	118
2015/11/11	97.7	31	983,300	14,460	614	5.60	0.0562	315	1.73	1160	1.54	10.9	-53	-6.7	-603	119
2015/12/8	96.6	28	981,700	17,360	474	10.4	0.0424	272	1.63	225	1.47	1.83	-49	-6.1	-608	114
2016/1/8	96.7	29	982,300	16,700	583	6.90	0.0478	231	1.10	188	1.37	0.381	-63	-8.7	-595	129
2016/1/28	97.9	29	979,900	18,900	656	11.3	0.0627	268	0.710	241	1.86	0.699	-53	-6.9	-609	114

Table 2 (continued)

Date yy/mm/dd	Temp °C	*CO ₂ /H ₂ S Molar ratio	H ₂ O μmol/ mol	CO ₂ μmol/ mol	H ₂ S μmol/ mol	SO ₂ μmol/ mol	He μmol/ mol	H ₂ μmol/ mol	O ₂ μmol/ mol	N ₂ μmol/ mol	CH ₄ μmol/ mol	Ar μmol/ mol	δD _{SNOW} H ₂ O	δ ¹⁸ O _{SNOW} H ₂ O	δD _{SNOW} H ₂	**AET °C
2016/2/15	95.5	29	990,700	8510	454	6.20	0.0434	209	0.106	154	1.20	0.347	-50	-64	-607	114
2016/3/2	95.5	28	982,600	16,320	647	15.7	0.0482	211	0.035	193	1.44	0.673	-55	-74	-611	113
2016/4/8	97.6	28	985,000	14,090	561	13.7	0.0459	207	0.000	174	1.41	0.620	-50	-68	-609	113
2016/5/13	97.3	26	986,300	12,830	559	8.10	0.0388	169	0.319	160	1.23	0.708	-51	-69	-605	116
2016/6/3	97.6	23	986,300	12,820	578	1.60	0.0376	178	0.343	161	1.32	0.503	-51	-66	-606	116
2016/7/5	97.4	23	983,700	15,110	744	3.50	0.0484	204	0.089	203	1.91	0.640	-57	-77	-610	114
2016/8/5	96.9	26	989,600	9520	582		0.0415	173	0.019	154	1.50	0.451	-51	-67	-607	115
2016/9/5	97.4	21	989,200	10,070	503	8.00	0.0305	120	0.018	129	1.30	0.443	-49	-63	-613	109
2016/10/7	97.2	22	989,000	10,190	422	10.6	0.0347	214	0.584	135	1.35	0.451	-51	-74	-615	109
2016/10/19	96.6	21	990,300	8960	445	13.5	0.0293	207	0.568	115	1.19	0.387	-47	-63	-610	111
2016/11/4	97.5	22	988,800	10,300	490	7.70	0.0369	231	1.56	146	1.44	0.579	-49	-58	-605	116
2016/12/7	97.2	21	989,800	9370	396	9.00	0.0369	258	0.064	150	1.58	1.15	-48	-57	-612	109
2017/1/11	96.8	22	982,400	16,360	766	16.7	0.0529	257	0.033	207	2.49	0.663	-51	-66	-611	112
2017/2/6	96.7	20	976,400	21,970	1010	13.0	0.0579	361	0.026	287	3.36	1.06	-59	-75	-618	108
2017/3/9	96.7	21	980,700	17,670	1100	14.2	0.0552	239	0.236	230	2.67	1.07	-56	-73	-626	101
2017/4/10	92.4	20	983,000	15,160	1380	44.9	0.0472	154	0.434	222	2.76	1.07	-56	-75	-625	101
2017/5/10	97.2	23	984,000	14,730	905	5.40	0.0505	196	0.046	203	2.55	0.674	-57	-74	-622	104
2017/6/10	96.5	21	975,300	22,640	1470	63.3	0.0772	227	0.000	307	3.81	1.14	-58	-74	-604	120
2017/7/4	97.6	23	983,100	15,820	744	4.60	0.0461	107	0.168	203	2.17	0.696	-56	-70	-589	132
2017/8/1	96.8	26	978,500	20,250	844	18.3	0.0653	139	0.121	278	2.47	0.820	-56	-74	-584	137
2017/9/2	96.4	26	970,400	28,060	1000	17.2	0.0858	155	0.166	364	2.96	1.12	-58	-77	-606	118
2017/10/4	96.8	25	973,000	25,220	1010	25.0	0.0716	73.5	26.7	612	2.48	6.49	-55	-71	-599	123
2017/11/7	97.2	28	983,800	15,140	548	7.50	0.0473	255	0.000	215	1.64	0.599	-54	-69	-618	107
2017/12/5	97.0	27	986,500	12,520	548	30.7	0.0390	258	0.000	186	1.51	0.547	-49	-60	-605	116
2018/1/9	96.4	29	988,300	10,910	435	3.50	0.0361	165	0.107	148	1.32	0.403	-46	-5.1	-585	132
2018/2/5	96.7	24	979,200	19,670	775	7.20	0.0604	126	0.040	262	2.40	0.954	-58	-7.6	-589	133

*Ratio determined by "Gas detector tubes system"

**Apparent equilibrium temperature defined between δD of H₂O and H₂

Table 3 Chemical and isotopic composition of fumarolic gas sampled at the point C in Owakudani geothermal area, Hakone volcano, Japan

Date yy/mm/dd	Temp °C	H ₂ O μmol/ mol	CO ₂ μmol/ mol	H ₂ S μmol/ mol	SO ₂ μmol/ mol	HCl μmol/ mol	He μmol/ mol	H ₂ μmol/ mol	O ₂ μmol/ mol	N ₂ μmol/ mol	CH ₄ μmol/ mol	Ar μmol/ mol	δD _{SMOW} H ₂ O	δ ¹⁸ O _{SMOW} H ₂ O	δD _{SMOW} H ₂	*AET °C
2015/12/25	131.9	988,200	5640	2050	1730	2360	0.0163	4.68	0.763	64.3	0.195	0.763	-30	1.4	-307	482
2016/6/7	124.4	991,100	4630	2240	1120	850	0.0148	1.88	0.210	52.2	0.161	0.151	-31	0.6	-254	597
2017/8/7	123	979,300	17,050	1,340	2,070	0	0.0488	1.32	1.55	188	0.0806	1.19	-29	1.0	-254	597

*Apparent equilibrium temperature defined between δD of H₂O and H₂

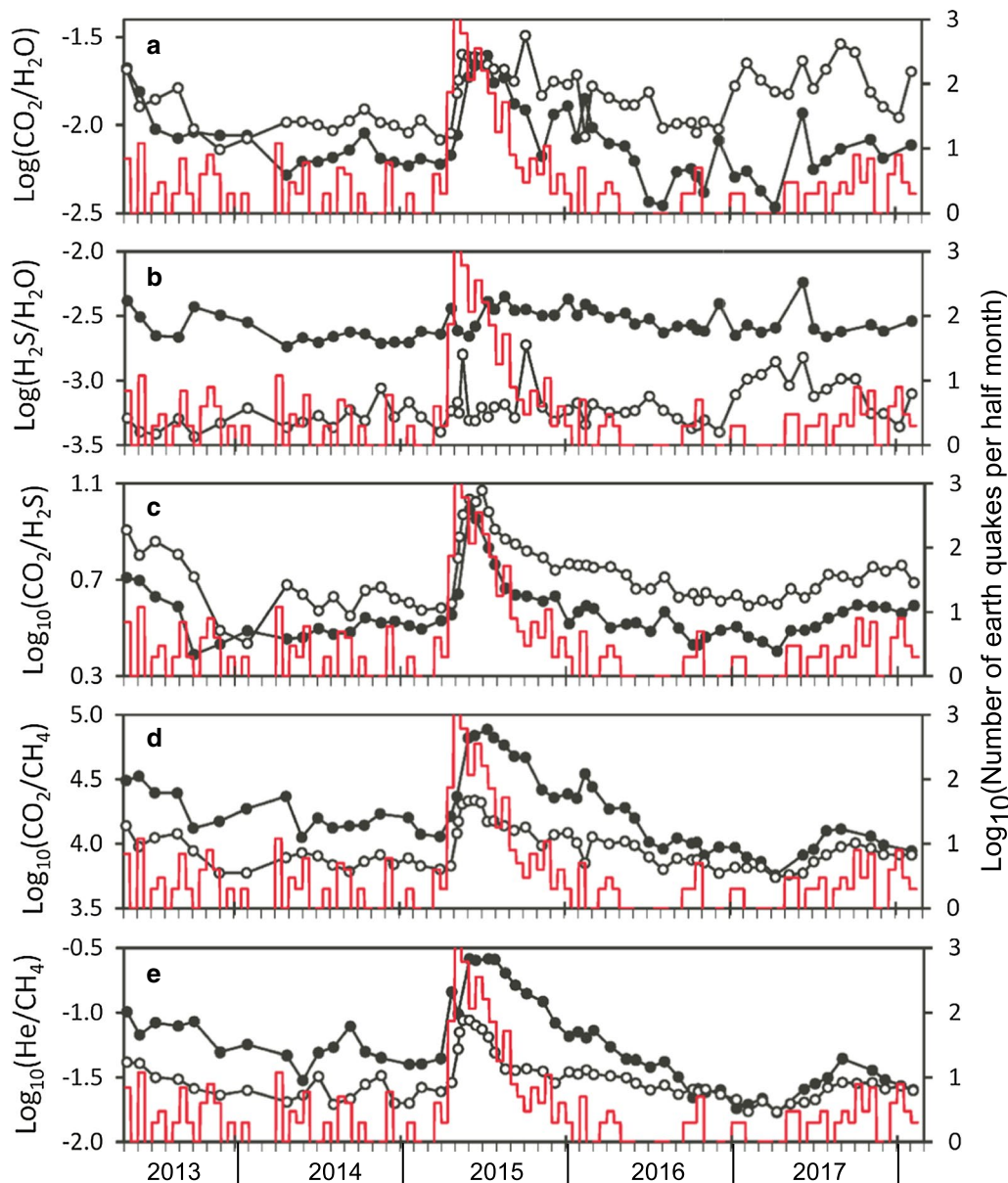


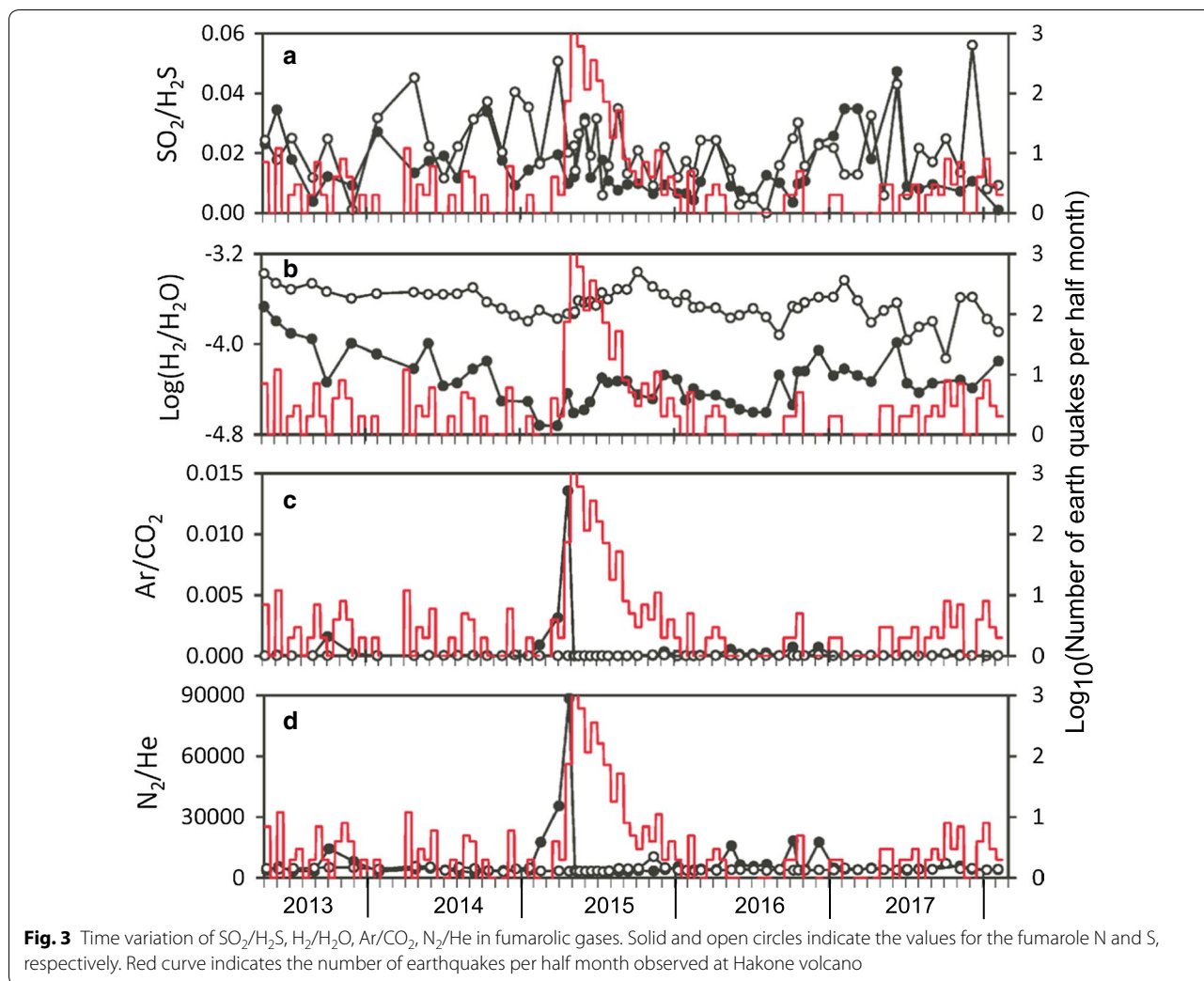
Fig. 2 Time variation of CO₂/H₂O, H₂S/H₂O, CO₂/H₂S, CO₂/CH₄ and He/CH₄ in fumarolic gases. Solid and open circles indicate the values for the fumarole N and S, respectively. Red curve indicates the number of earthquakes per half month observed at Hakone volcano

$$C_{N_2}^* = C_{N_2} - \left(\frac{78.08}{20.95} \right) C_{O_2}, \tag{3}$$

where C_i is the concentration of i in fumarolic gas and C_i^* is the corrected concentration eliminating the effect of direct air contamination. In the equations, it was assumed that the fumarolic gas does not include O₂ originally, and the O₂ contaminated in fumarolic gas accompanied atmospheric N₂ and Ar with the equivalent air abundance. It should be noted that the above correction

does not account for O₂ lost in the oxidation of reduced S in solution.

In general, the SO₂/H₂S ratio is a useful parameter for evaluating volcanic activity, as it tends to increase when volcanic activity was elevated (e.g., Ossaka et al. 1980). With some fluctuation, SO₂/H₂S ratio of N and S was < 0.06 over the whole duration of this study (Fig. 3a), being a contrast to the SO₂/H₂S ratio at C as high as 0.5 to 1.5 (Table 3). The H₂/H₂O ratio shows a weak correlation with the number of earthquakes; it started to



increase slightly after May 2015; then, it maximized in the late of 2015 (Fig. 3b).

The Ar/CO_2 and N_2/He ratios show a sharp increase a few months prior to the earthquake swarm in May 2015. Actually, Ar/CO_2 and N_2/He ratios maximized on April, 24, 2015, which was 2 days before the start of earthquake swarm. On May, 8, 2015, those ratios returned to the normal levels. It should be noticed that those precursory increases only happened at fumarole N. No increase was detected at S fumarole.

The time variation in δD of H_2O , $\delta^{18}\text{O}$ of H_2O , δD of H_2 and the apparent equilibrium temperature (AET) are shown in Fig. 4. The AET was calculated between δD of H_2O and δD of H_2 based on the following equation (Richet et al. 1977),

$$\text{AET} = \left(4.474 \times 10^{-12}x^2 + 3.482 \times 10^{-9}x + 9.007 \times 10^{-8} \right)^{-0.5} - 273.15 \quad (4)$$

where

$$x = 1000 \ln \left\{ \frac{\delta\text{D}(\text{H}_2\text{O}) + 1000}{\delta\text{D}(\text{H}_2) + 1000} \right\} \quad (5)$$

The averaged H_2 concentration in the gas of N, S and C is 2.6, 55 and 233 $\mu\text{mol}/\text{mol}$, respectively. The depth of the borehole, from which the gas of C is discharging, is 500 m below the surface. Therefore, the most of H_2 in the gas of N and S is thought to be formed in the crust shallower than -500 m to surface. The δD of H_2 in the gas of C is much higher than the ratio of the gas N and S (see Tables 1, 2 and 3), consistent with the above estimation on H_2 formation. The AET calculated between the δD of H_2O and H_2 means the temperature of crust shallower than -500 m to surface. The δD and $\delta^{18}\text{O}$ of H_2O decreased significantly a few months prior to the start of earthquake swarm in May 2015 (Fig. 4a, b) at

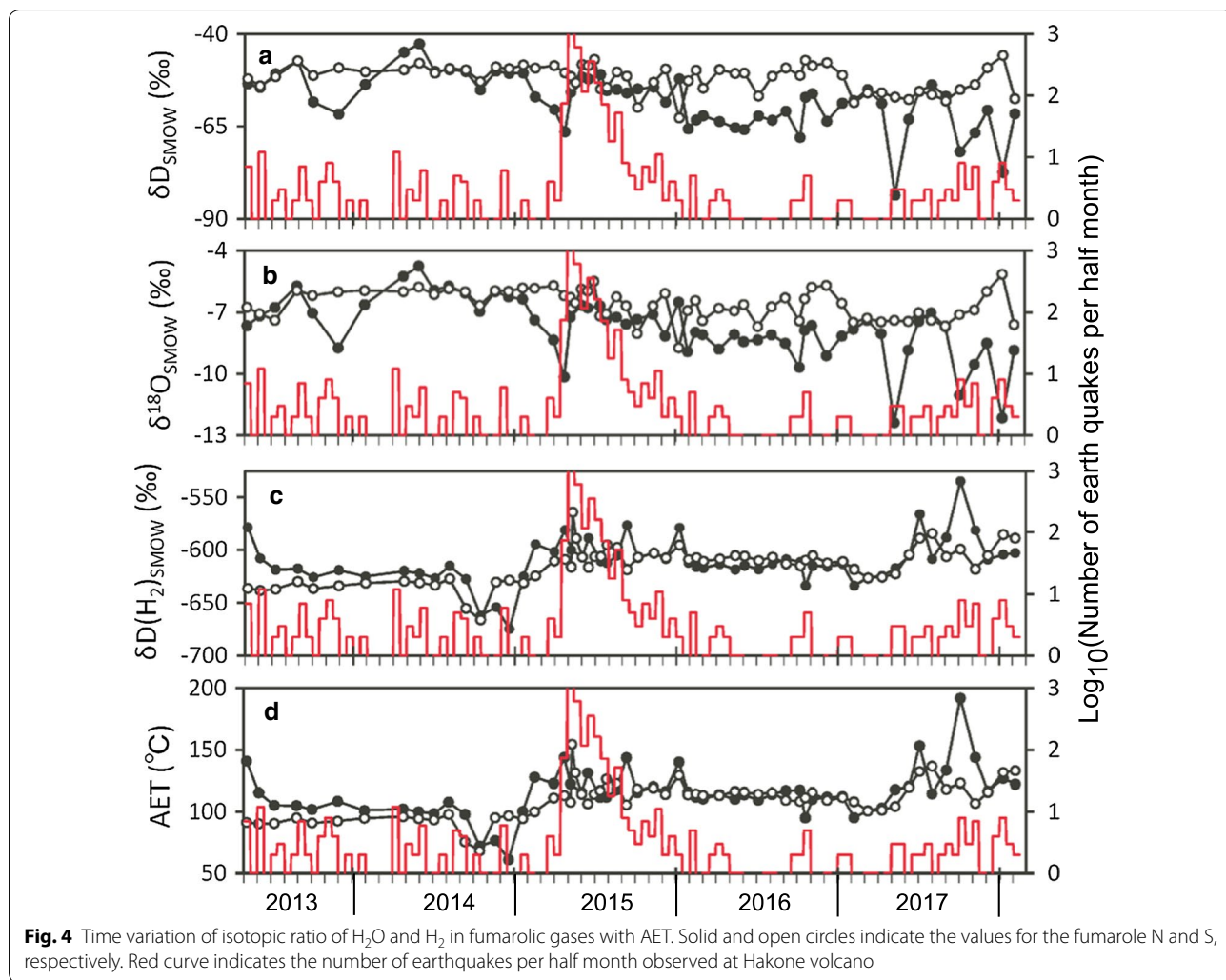


Fig. 4 Time variation of isotopic ratio of H₂O and H₂ in fumarolic gases with AET. Solid and open circles indicate the values for the fumarole N and S, respectively. Red curve indicates the number of earthquakes per half month observed at Hakone volcano

N fumarole. A similar decrease was observed in 2017 at fumarole N, whereas no decrease was observed at fumarole S.

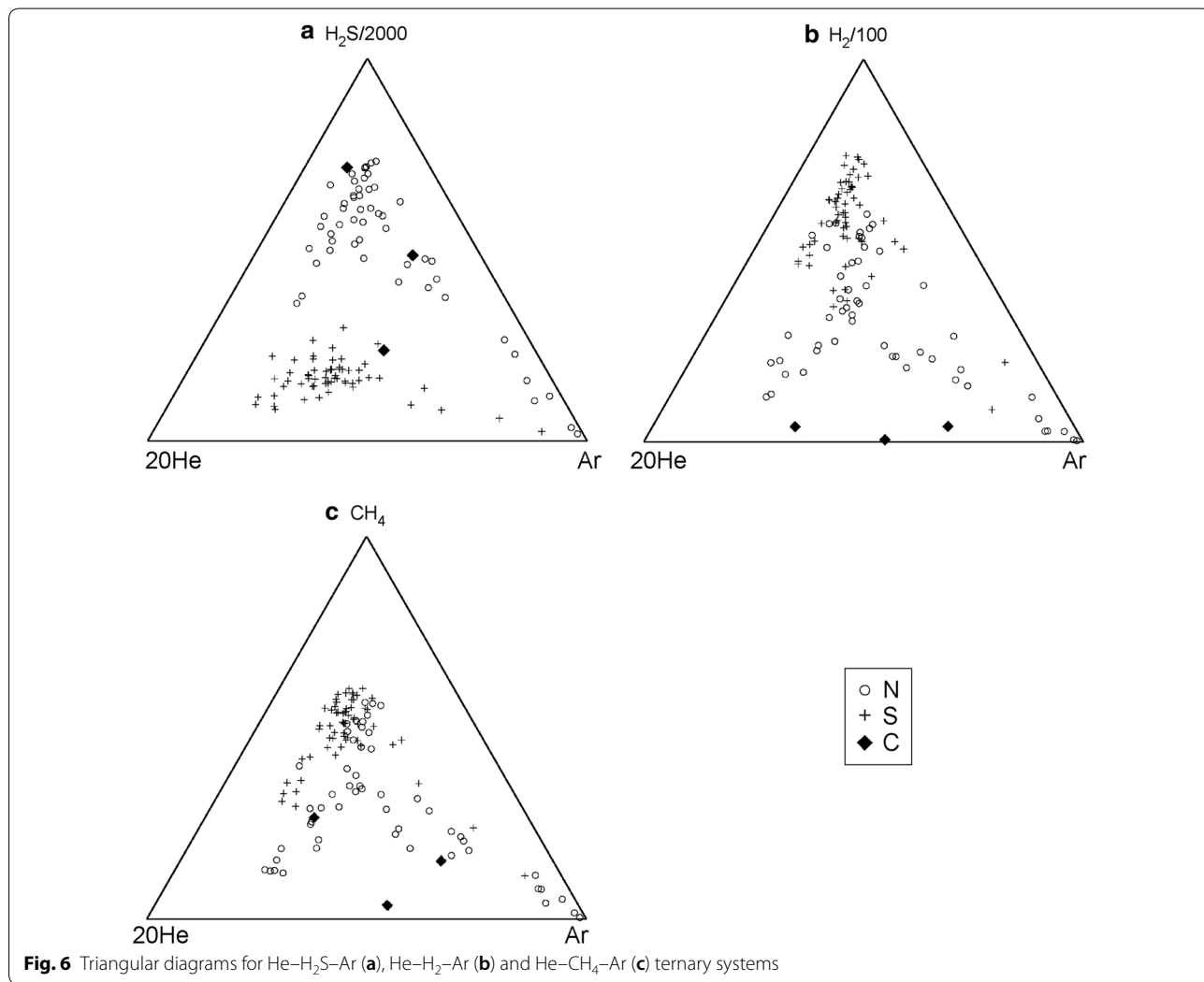
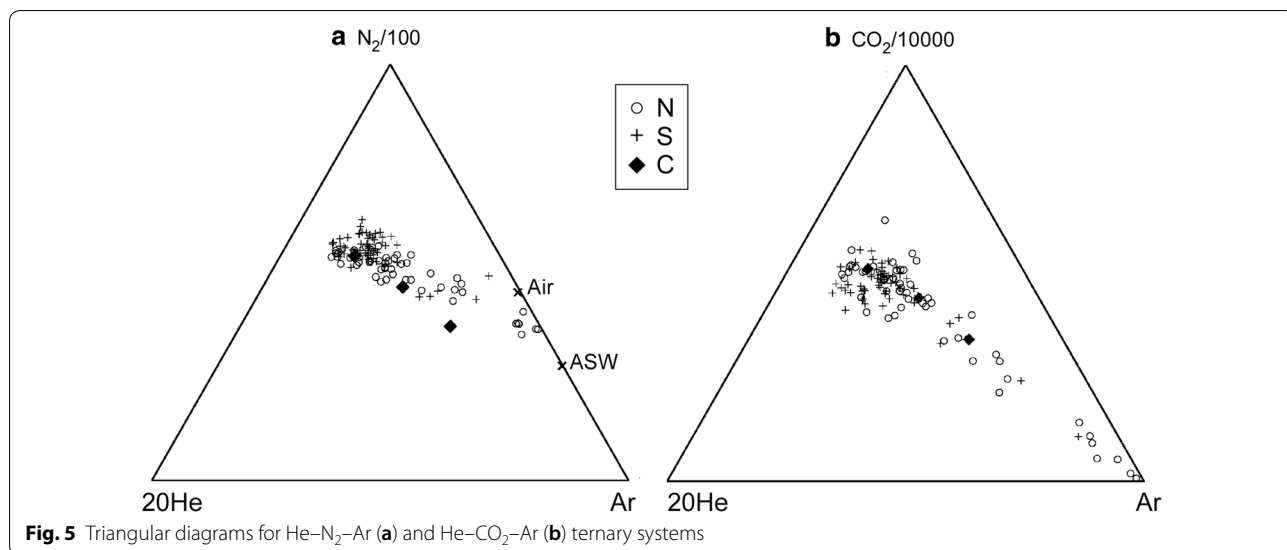
The δD of H₂ and AET were stable over the whole duration of this study with the exception of two periods. In September to December 2014, those values significantly decreased relative to normal level (Fig. 4c, d). A slight decrease was also observed in March and April in 2017. It should be noticed that the both decreases happened almost simultaneously at N and S fumaroles.

Discussion

We try to group the components in fumarolic gas by use of triangular diagrams (Fig. 5). The He–N₂–Ar ternary diagram shows a linear distribution of data points, suggesting two common-end members in fumarolic gases N, S and C. The end member with high He/Ar and N₂/Ar ratios is estimated to be the magmatic component which

is ubiquitous at the volcanoes on subduction zone (Kita et al. 1993; Giggenbach 1997). Another end member with low He/Ar and N₂/Ar ratios could be air or ASW. The ASW is the atmospheric components saturated in water at 15 °C. A similar feature also found in the diagram for He–CO₂–Ar system (Fig. 5), suggesting the fumarolic gases N, S and C, contains a common magmatic component.

In Fig. 6a–c, respectively, for He–H₂S–Ar, He–H₂–Ar and He–CH₄–Ar, the distributions of data points are different from the distribution in Fig. 5. No definite value can be found in H₂S/He, H₂/He and CH₄/He ratios for non-atmospheric end member, suggesting H₂S, H₂ and CH₄ belongs to a group different from the magmatic component. As explained by Giggenbach (1987), the reduced molecules group, H₂S, H₂ and CH₄, are originating in hydrothermal system. Those molecules are generated by the reaction between magmatic gas and Fe²⁺



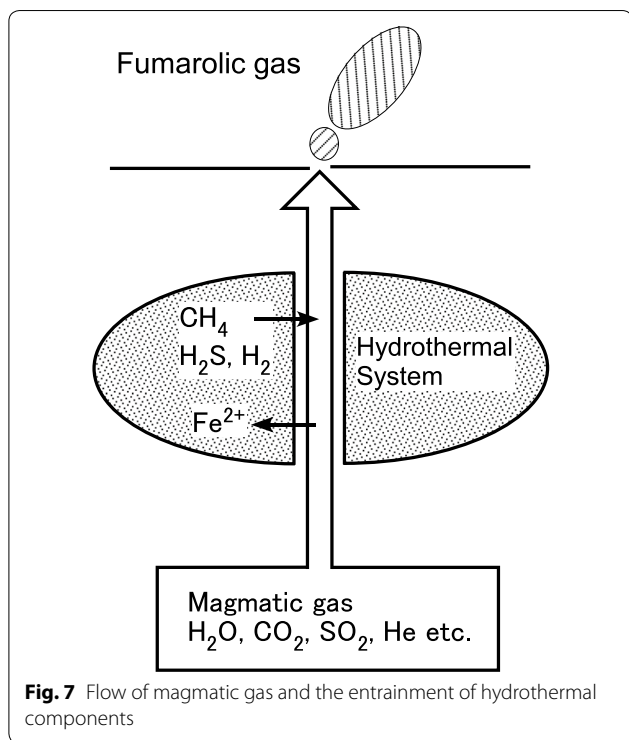
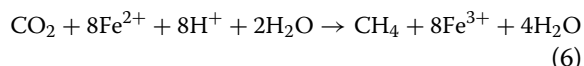


Fig. 7 Flow of magmatic gas and the entrainment of hydrothermal components

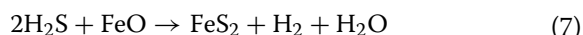
contained in crustal rock. For example, the following reaction can be written for the formation of CH₄.



The behavior of magmatic gas and hydrothermal fluid is illustrated in Fig. 7. The magmatic gases such as CO₂ and SO₂ are converted to CH₄ and H₂S in hydrothermal system due to the reduction by Fe²⁺ in crustal rock. The reduced

components are stored in hydrothermal system and entrained by the flow of magmatic gas. The fumarolic gas discharged at the surface contains both components. When the flux of magmatic gas increases, if the flux of hydrothermal entrainment is constant, the magmatic/hydrothermal component ratios such as CO₂/CH₄ and CO₂/H₂S are expected to be elevated. This situation is consistent with the observed changes of CO₂/H₂O, CO₂/H₂S, CO₂/CH₄ and He/CH₄ ratios in May 2015 (Fig. 2a, c–e). Actually, the flux of hydrothermal component entrained in the flow of magmatic component would not be constant. However, the variation of the flux by entrainment may be much smaller than the variation in the magmatic component flow.

Substituting He by CH₄, the triangular diagrams of Fig. 6 can be converted to Fig. 8, where definite non-atmospheric end members can be found for H₂S/CH₄ ratio (Fig. 8a). It should be noticed that the H₂S/CH₄ ratio is similar for N and C. The H₂S/CH₄ ratio for S is much lower than the ratio for N and C. The geothermal area Ky, where fumarole S is located, was developed newly after the earthquake swarm in 2001. Before 2001, the place of Ky was densely forested. After 2001, the trees in Ky area were completely devastated due to geotherm. The averaged H₂S concentration in the gas of N, S and C is 2800, 660 and 1900 μmol/mol, respectively. The H₂S concentration of the gas S is much lower than that of N and C. The reason for the low H₂S/CH₄ ratio of S may be the removal of H₂S along the reaction with Fe in crustal rock or soil as,



Since Ky area has been developed recently, the crustal rock or soil contacting volcanic gas flow may contain plenty of Fe. The reaction (7) at Ky area may be effective relative to Ow area. The averaged CH₄ concentration

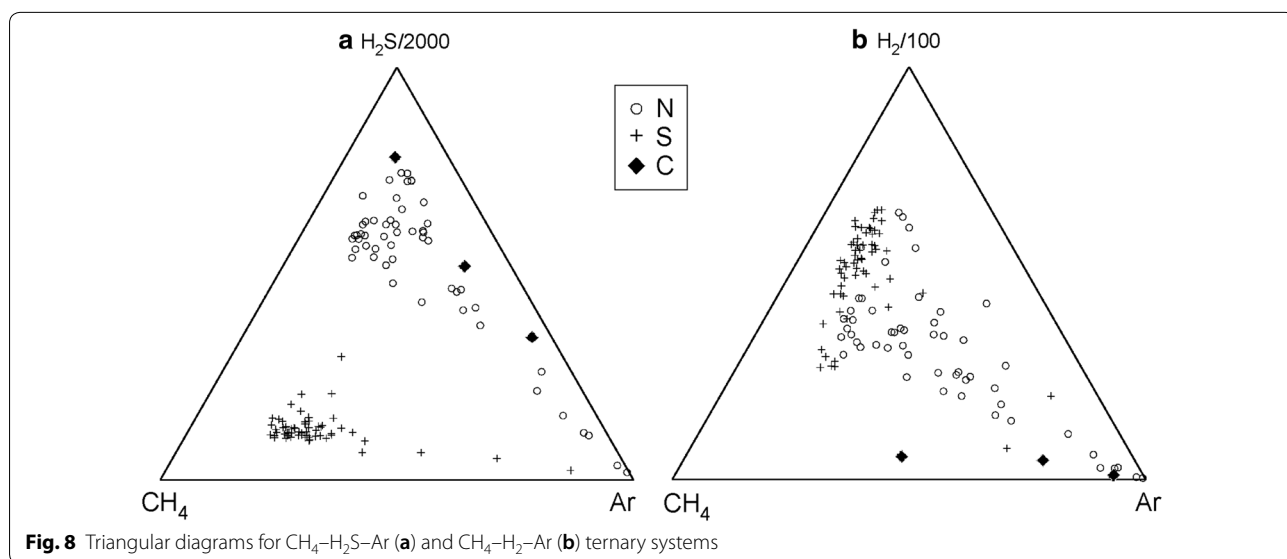
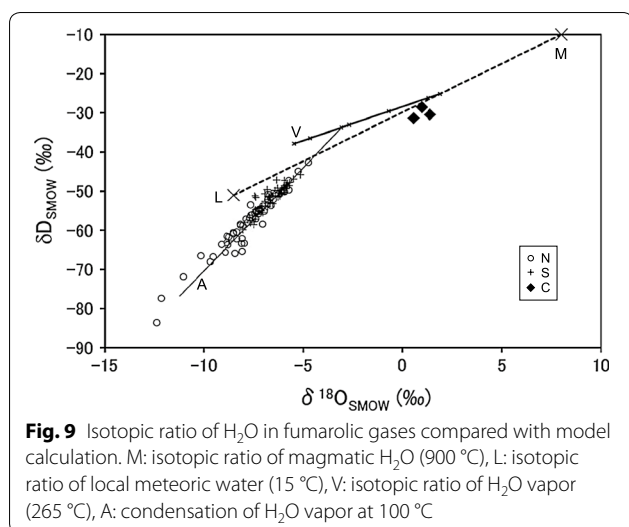


Fig. 8 Triangular diagrams for CH₄-H₂S-Ar (a) and CH₄-H₂-Ar (b) ternary systems



in the gas of N, S and C is 0.49, 1.6 and 0.15 $\mu\text{mol/mol}$, respectively. The concentration in the gas S is higher than that of N and C. Because the Ky area is the newly developed geothermal area, the shallow crust is expected to contain much organic matter. A part of CH₄ in the gas of S originates in the thermogenic component (Taran and Giggenbach, 2003). The high CH₄/H₂S ratio of the gas S relative to N and C seems to be brought by the two effects, the removal of H₂S and the addition of thermogenic CH₄.

Figure 8b shows the existence of non-atmospheric end member for H₂/CH₄ ratio although the range of ratio is much wider than H₂S/CH₄ ratio in Fig. 8a. It should be noticed that the H₂/CH₄ ratio for fumarole C is significantly lower than that for fumarole N and S. Methane is a component generated in the deep part of hydrothermal system (Giggenbach 1987). The fumarole C is the newly created crater in 2015. The fumarolic gas of C represents the fluid which is transported to surface bypassing the shallow part of hydrothermal system. Therefore, the abundant H₂ contained in N and S fumarolic gases would be generated in shallow part of hydrothermal system.

The stable isotopic ratio of H₂O in fumarolic gas enables us to estimate the fluid evolution. As shown in Fig. 9, the data points are distributed linearly on δD versus $\delta^{18}\text{O}$ plane. In order to explain the distribution, a model calculation was carried out. The method of calculation has been demonstrated by Ohba et al. (2011). The parameters used in the calculation are summarized in Table 4. For the isotopic ratio of H₂O of magmatic gas, the typical values for andesitic volcano on subduction zone (Giggenbach 1992) are assigned. In the model calculation, a high enthalpy magmatic gas (M in Fig. 9) mixed with a low enthalpy meteoric water (L in Fig. 9). As the result of mixing, a vapor phase (V in Fig. 9) and thermal water

Table 4 Parameters used in the model calculation of vapor phase in terms of isotopic ratio of H₂O and CO₂/H₂O ratio

Parameter	Value	Unit
Temperature of magmatic gas	900	°C
Temperature of local meteoric water	15	°C
Temperature of vapor and thermal water	265	°C
Temperature of vapor condensation	100	°C
δD of H ₂ O in magmatic gas	-10	‰ to SMOW
$\delta^{18}\text{O}$ of H ₂ O in magmatic gas	8.0	‰ to SMOW
δD of H ₂ O in local meteoric water	-51	‰ to SMOW
$\delta^{18}\text{O}$ of H ₂ O in local meteoric water	-8.5	‰ to SMOW
CO ₂ /H ₂ O ratio of magmatic gas (high)	0.013	Molar ratio
CO ₂ /H ₂ O ratio of magmatic gas (low)	0.0045	Molar ratio

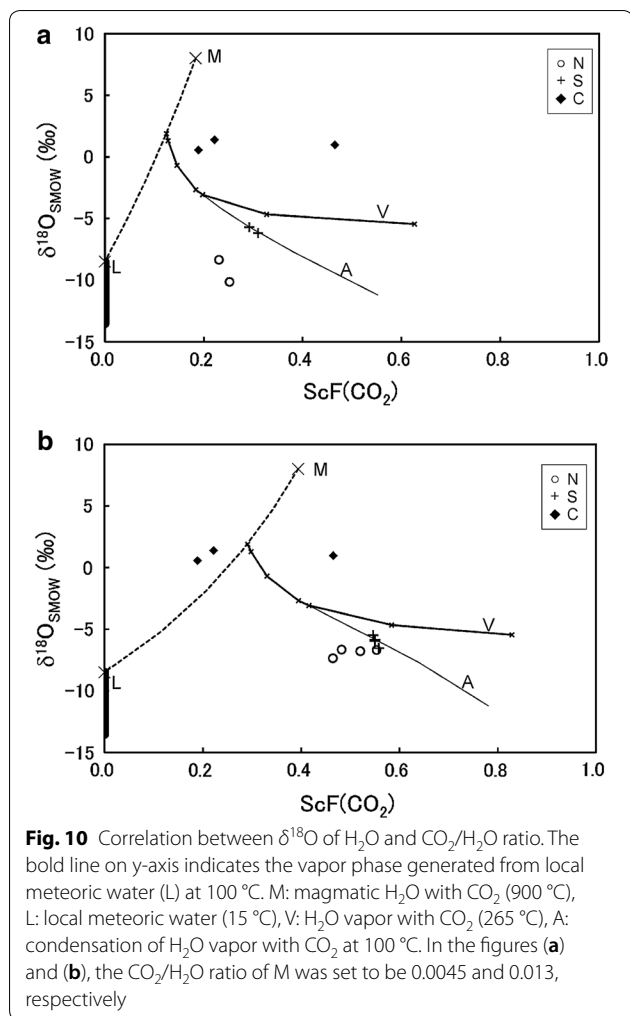
phase were generated. Their temperature was set to be 265 °C, which is the average apparent equilibrium temperature assuming the equilibrium of,



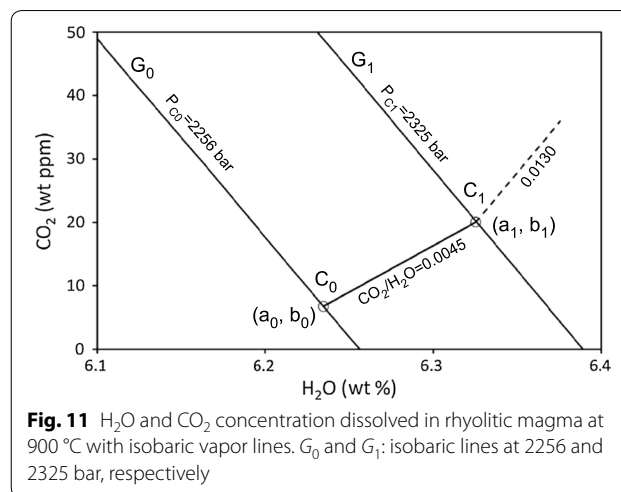
for the chemical composition of gas from borehole of Ow geothermal area (Ohba et al. 2011). During the mixing of M and L, the conservation of enthalpy, isotopic ratio and CO₂/H₂O ratio were assumed. After the mixing, vapor–liquid separation occurs. The conservation of enthalpy, isotopic ratio and CO₂/H₂O ratio was assumed also during the separation step, where the isotopic fractionation and CO₂/H₂O distribution took place between vapor phase (V) and liquid phase. The vapor phase (V) could suffer a cooling and a removal of condensed water. During the condensation, the isotopic composition of vapor moves along the line A. The temperature was set to be 100 °C during the condensation. The observed decrease in the isotopic ratio of H₂O can be attributed to a condensation of H₂O vapor. The correctness of the above model is supported by the data points for fumarole C, which were plotted near the cross-point between the line V and the line M–L. In the model calculation, at the cross-point, the amount of thermal water is zero. The fumarolic gas of C contains HCl (Table 3), suggesting the amount of liquid phase coexisting with fumarolic gas C was limited. The fumarolic gas C is interpreted to be the gas phase of direct mixing between magmatic gas (M) and meteoric water (L).

In the model calculation, CO₂/H₂O ratio of fumarolic gas can be correlated with isotopic ratio of H₂O. In Fig. 10a, b, the result of model calculation is compared with observed fumarolic gas composition. In the diagrams, CO₂/H₂O ratio is converted to the scaled CO₂ fraction (ScF) as

$$\text{ScF}(\text{CO}_2) = \frac{100C_{\text{CO}_2}}{C_{\text{H}_2\text{O}} + 100C_{\text{CO}_2}}, \quad (9)$$



where C_{CO_2} and $C_{\text{H}_2\text{O}}$ are the concentration of CO_2 and H_2O in gases, respectively. The difference between Fig. 10a and b is the $\text{CO}_2/\text{H}_2\text{O}$ ratio of magmatic gas (M) and the period of fumarolic gas. In Fig. 10a, $\text{CO}_2/\text{H}_2\text{O}$ ratio of M is 0.0045 and the data of fumarolic gases in March and April 2015 are plotted when the $\text{CO}_2/\text{H}_2\text{O}$ ratio was low (Fig. 2a). In Fig. 10b, $\text{CO}_2/\text{H}_2\text{O}$ ratio of M is 0.013. The fumarolic gas N in June and July 2015 and S in May and June 2015 are plotted. In the above period, the $\text{CO}_2/\text{H}_2\text{O}$ ratios of N and S were maximized (Fig. 2a). The $\text{ScF}(\text{CO}_2)$ of fumarole N in Fig. 10a, b is separated from the line A. The separation could be explained by the addition of vapor phase originating in local meteoric water (L). The composition of the vapor phase is indicated on the bold line on the y-axis. Figure 10a, b suggests that the $\text{CO}_2/\text{H}_2\text{O}$ ratio of magmatic gas was high as 0.013 when the number of earthquake increased in May 2015, and low as 0.0045 before the start of earthquake swam (Fig. 2a).



The above variation in $\text{CO}_2/\text{H}_2\text{O}$ ratio is consistent with the magma sealing model (Fournier 1999). Accepting the estimation by Yukutake et al. (2015), the depth of degassing magma and the pressure were assumed to be -10 km and 2256 bar, respectively. A degassing magma should be saturated in term of H_2O and CO_2 . Therefore, the H_2O and CO_2 concentration in magma is located on the isobaric line G_0 of Fig. 11. The isobaric line was drawn by use of the PC software VolatileCalc (Newman and Lowenstern 2002). For the calculation of isobaric line, the temperature and composition of magma were assumed to be 900 °C and rhyolitic (Tsujiyama et al. 2017), respectively. On the line G_0 , the $\text{CO}_2/\text{H}_2\text{O}$ ratio of gas phase can be calculated by VolatileCalc at any point, assuming equilibrium distribution of H_2O and CO_2 between magma and gas phase. VolatileCalc gave 0.0045 for the $\text{CO}_2/\text{H}_2\text{O}$ ratio of gas phase at the point C_0 . The value 0.0045 is the $\text{CO}_2/\text{H}_2\text{O}$ ratio of magmatic gas (M) when the number of earthquake was low. The H_2O and CO_2 concentration at the point C_0 was 6.235 wt% (a_0) and 6.75 wt ppm (b_0), respectively. The above concentration represents the portion of magma equilibrated with gas phase, namely the inner surface of bubbles generated in degassing magma. We assign a_1 and b_1 , respectively, to the bulk concentration of H_2O and CO_2 in magma. The point C_1 defined by a_1 and b_1 should be located on the line with 0.0045 of slope starting from the point C_0 (Fig. 11). Fournier (1999) proposed the magma sealing model explaining the episodic volcanic activity without magma intrusion. If the sealing zone restricts the emission of degassed gas, magma is compressed by the gas itself. When the sealing zone is broken, the gas stored within the sealing zone is supplied to hydrothermal system producing earthquakes and activation of fumarolic activity or phreatic eruption. Therefore, the $\text{CO}_2/\text{H}_2\text{O}$ ratio of magmatic gas, 0.013,

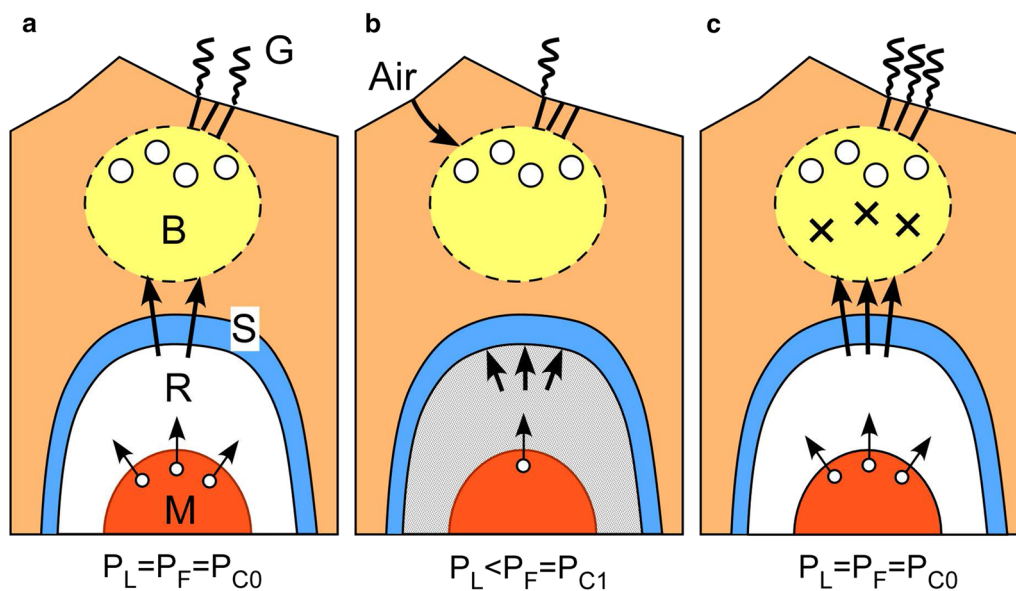


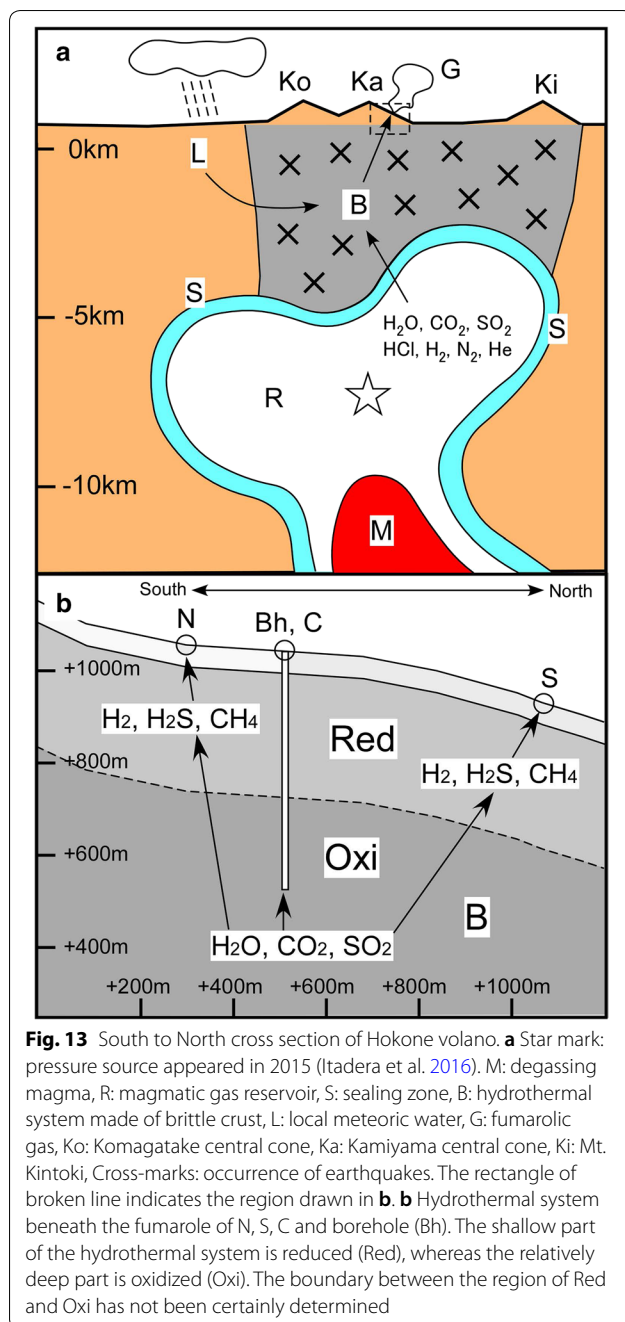
Fig. 12 Sequence at Hakone volcano before and after the earthquake swarm in May 2015. **a** Normal situation represented by the period in 2014. M: degassing magma, R: magmatic gas reservoir, S: sealing zone, B: hydrothermal system made of brittle crust, G: fumarolic gas, P_L : lithostatic pressure, P_F : magmatic gas pressure, P_{C0} and P_{C1} : gas pressure equilibrated with magma the composition of which is C_0 and C_1 in Fig. 11. **b** Sealing zone is restricting the magmatic gas transport to hydrothermal system, corresponding to the period in few months prior to May 2015. Air invasion was allowed into hydrothermal system. **c** Break of sealing zone in May 2015. A large number of earthquakes (cross-marks) happened in hydrothermal system

during the earthquake swarm can be attributed to the gas phase when magma was compressed by gas itself. Assuming that CO_2/H_2O ratio is 0.013 in the gas equilibrium, the magma at the point C_1 , a_1 and b_1 was calculated to be 6.33 wt% and 20.04 wt ppm, respectively. The isobaric line for 2325 bar is drawn on the point C_1 .

The sequence of events over the earthquake swarm in May 2015 is summarized schematically in Fig. 12. In 2014, a steady degassing of magma and the transport of magmatic gas to hydrothermal system were kept (Fig. 12a). In this period, the magmatic gas pressure P_F equals to the lithostatic pressure P_L . The P_F equals to P_{C0} which is the gas pressure equilibrated with the inner surface of bubbles in magma. In February 2015 until April 2015, the magma sealing took place (Fig. 12b), restricting the emission of magmatic gas resulting in the pressurization of magma by gas itself. At the end of the period, P_F was elevated up to P_{C1} . During the magma sealing, the supply of magmatic gas to hydrothermal system was restricted. The fluid pressure in hydrothermal system may be decreased, and enthalpy of hydrothermal system may be also decreased. The pressure decrease could cause an invasion of air, which elevated Ar/CO_2 and N_2/He ratios prior to the earthquake swarm (Figs. 3c, d, 12b). The enthalpy decrease could prompt the condensation of H_2O vapor, which reduced the isotopic ratio of H_2O (Fig. 4a, b). In May 2015, the sealing zone was broken

(Fig. 12c). The magmatic gas with high CO_2/H_2O ratio was supplied to hydrothermal system as a surge. The supply of magmatic gas lifted the fluid pressure and produced large number of earthquake and a small phreatic eruption in June 2015.

Based on the structure estimated by Yukutake et al. (2015) and the discussions in this study, the magmatic hydrothermal system of Hakone volcano is illustrated in Fig. 13a. The magmatic gas is supplied by the degassing magma (M). The gas contains H_2O , CO_2 , SO_2 , HCl , N_2 , H_2 and He . A magmatic gas reservoir (R) is developed above the degassing magma (Yukutake et al. 2015), and it was surrounded by a sealing zone (S). According to Itad- era et al. (2016), a pressure source (star mark in Fig. 13a) is located at -8.4 km below the sea level and beneath Ka, which produced the inflation of volcanic body in May 2015. The pressure source is located within the magmatic gas reservoir (R). Through the sealing zone, magmatic gas is transported to the hydrothermal system made of brittle crust (B). Most of SO_2 and a part of CO_2 in the magmatic gas are converted to H_2S and CH_4 in the hydrothermal system with the reaction of Fe^{2+} contained in crustal rock within the crust shallower than -500 m (Fig. 13b). The magmatic gas was discharged as fumarolic gas N and S with the entrainment of hydrothermal components such as H_2S and CH_4 .



Conclusions

Sharp increases in the components ratios such as $\text{CO}_2/\text{H}_2\text{O}$, $\text{CO}_2/\text{H}_2\text{S}$, CO_2/CH_4 and He/CH_4 were observed at the fumarolic gas on Hakone volcano synchronized with the earthquake swarm in 2015. The increases could be explained by the dominance of magmatic component relative to hydrothermal component. The $\text{CO}_2/\text{H}_2\text{O}$ ratio of magmatic gas was 0.0045 before the earthquake swarm. It increased to 0.013 during the

earthquake swarm. The increase in $\text{CO}_2/\text{H}_2\text{O}$ ratio can be explained by the pressurization of magma caused by magma sealing. The magma pressure increased from 2256 to 2325 bar, consistent with the increase in the $\text{CO}_2/\text{H}_2\text{O}$ ratio. The bulk H_2O and CO_2 concentration in magma were estimated to be 6.33 wt% and 20.0 wt ppm, respectively assuming the temperature of magma is 900 °C and the composition of magma is rhyolitic. Prior to the earthquake swarm in May 2015, sharp increase in Ar/CO_2 and N_2/He ratios was observed at the fumarolic gas in Ow geothermal area. The increase could be explained by the invasion of air in hydrothermal system. A definite decrease in the isotopic ratio of H_2O in the fumarolic gas in Ow geothermal area was observed prior to the earthquake swarm in May 2015. The decrease could be explained by the partial condensation of H_2O vapor probably due to the enthalpy loss in hydrothermal system beneath Ow geothermal area. It should be noticed that the above changes prior to the earthquake swarm were not observed in the fumarolic gas S in Ky geothermal area.

Abbreviations

AET: apparent equilibrium temperature; ASW: atmospheric components saturated in water; GC: gas chromatograph; HSRI: Hot Springs Research Institute of Kanagawa Prefecture; JMA: Japan Meteorological Agency; Ka: Kamiyama; Ko: Komagatake; Ky: Kamiyuba; Ow: Owakudani; R-gas: residual gas; SMOW: Standard Mean Ocean Water; So: Souzanzan; wt: weight.

Authors' contributions

TO drafted the manuscript. MY, KN, NN and YD sampled fumarolic gases and analyzed them. CS, MI and UT analyzed fumarolic gas samples. All authors read and approved the final manuscript.

Author details

¹ Tokai University, 4-1-1 Kitakaneme, Hiratsuka, Kanagawa 259-1291, Japan. ² Meteorological Research Institute, 1-1 Nagamine, Tsukuba, Ibaraki 305-0052, Japan. ³ Kanagawa Environmental Research Center, Shinomiya 1-3-39, Hiratsuka, Kanagawa 254-0014, Japan. ⁴ Graduate School of Environmental Studies, Nagoya University, Furo-cho, Chikusa-ku, Nagoya 464-8601, Japan. ⁵ Present Address: Center for Marine Research and Operation, Tokyo University of Marine Science and Technology, 4-5-7 Konan, Minato-ku, Tokyo 108-8477, Japan.

Acknowledgements

This work was supported by the Japanese Ministry of Education, Culture, Sports, Science and Technology, under grant of the Integrated Program for Next Generation Volcano Research and Human Resource Development in 2016 to 2017, also under its Earthquake and Volcano Hazards Observation and Research Program in 2015 to 2017. This work was supported by Japan Society for the Promotion of Science (JSPS) KAKENHI Grant Numbers 15K12485 in 2015 to 2017. This work was supported by the Earthquake Research Institute, The University of Tokyo Joint Usage/Research Program in 2015 to 2017. This work was supported by General Research Institute of Tokai University in 2016 to 2017. We sincerely thank the above fund providers for the support in this work. We also thank Nagoya group: Kosuke Ikeya and Fumiko Nakagawa for $\delta\text{D}(\text{H}_2)$ measurement.

Competing interests

The authors declare that they have no competing interests.

Availability of data and materials

The csv files for Tables 1, 2 and 3 will be stored in repositories.

Consent for publication

Not applicable.

Endnotes

None.

Ethics approval and consent to participate

Not applicable.

Funding

This work was supported by the Japanese Ministry of Education, Culture, Sports, Science and Technology under grant of the Integrated Program for Next Generation Volcano Research and Human Resource Development in 2016 to 2017. This work was supported by Japan Society for the Promotion of Science (JSPS) KAKENHI Grant Numbers 15K12485 in 2015 to 2017. This study was supported by the Ministry of Education, Culture, Sports, Science and Technology (MEXT) of Japan, under its Earthquake and Volcano Hazards Observation and Research Program in 2015 to 2017. This study was supported by the Earthquake Research Institute, The University of Tokyo Joint Usage/Research Program in 2015 to 2017. This work was supported by General Research Institute of Tokai University in 2016 to 2017.

Publisher's Note

Springer Nature remains neutral with regard to jurisdictional claims in published maps and institutional affiliations.

Received: 7 April 2018 Accepted: 15 April 2019

Published online: 25 April 2019

References

- Daita Y (2013) Temporal variation of the fumarolic gas composition during the swarm earthquake activity in Hakone volcano in 2013. *Bull Hot Spring Res Inst Kanagawa Prefect* 45:29–34 (in Japanese)
- Fournier RO (1999) Hydrothermal processes related to movement of fluid from plastic into brittle rock in the magmatic-epithermal environment. *Econ Geol* 94:1193–1212
- Giggenbach WF (1975) A simple method for the collection and analysis of volcanic gas samples. *Bull Volcanol* 39:132–145
- Giggenbach WF (1987) Redox processes governing the chemistry of fumarolic gas discharges from White Island, New Zealand. *Appl Geochem* 2:143–161
- Giggenbach WF (1992) Isotopic shifts in waters from geothermal and volcanic systems along convergent plate boundaries and their origin. *Earth Planet Sci Lett* 113:495–510
- Giggenbach WF (1997) The origin and evolution of fluids in magmatic-hydrothermal systems. In: Barnes HL (ed) *Geochemistry of hydrothermal ore deposits*, 3rd edn. Wiley, Hoboken
- Itadera K, Harada M, Yoshida A (2016) Relationship between ground tilts and earthquake swarms during the 2015 Hakone volcanic activity. *Bull Hot Spring Res Inst Kanagawa Prefect* 48:1–10 (in Japanese)
- Kita I, Nitta K, Nagao K, Taguchi S, Koga A (1993) Difference in N/Ar ratio of magmatic gases from northeast and southwest Japan: new evidence for different states of plate subduction. *Geology* 21:391–394
- Kobayashi M, Okuno M, Nakamura T (1997) 14C ages of pyroclastic-flow deposits from central cones on the western slope of old Somma of Hakone volcano, central Japan. *Bull Volcanol Soc Japan* 42:355–358 (in Japanese)
- Kuno H (1950) Geology of Hakone volcano and adjacent areas. Part-I. *J Fac Sci Univ Tokyo Sect II* 7:257–279
- Lee S, Ohba T, Yun SH, Yang K, Jeong HY (2016) Evaluation of sampling methods for sulfur speciation in volcanic gases. *Chem Geol* 438:123–133
- Mannen K (2008) Hakone Caldera: mode of formation, and role in present-day volcanism. *Res Rep Kanagawa Prefect Mus Nat Hist* 13:61–76 (in Japanese with English abstract)
- Mannen K, Yukutake Y, Kikugawa G, Harada M, Itadera K, Takenaka J (2018) Chronology of the 2015 eruption of Hakone volcano, Japan: geological background, mechanism of volcanic unrest and disaster mitigation measures during the crisis. *Earth Planets Space* 70:68. <https://doi.org/10.1186/s40623-018-0844-2>
- Newman S, Lowenstern JB (2002) VolatileCalc: a silicate melt–H₂O–CO₂ solution model written in Visual Basic for excel. *Comput Geosci* 28:597–604
- Ohba T, Daita Y, Sawa T, Taira N, Kakuage Y (2011) Coseismic changes in the chemical composition of volcanic gases from the Owakudani geothermal area on Hakone volcano, Japan. *Bull Volcanol* 73:457–469. <https://doi.org/10.1007/s00445-010-0445-9>
- Ossaka J, Ozawa T, Nomura T, Ossaka T, Hirabayashi J, Takaesu A, Hayashi T (1980) Variation of chemical compositions in volcanic gases and waters at Kusatsu-Shirane volcano and its activity in 1976. *Bull Volcanol* 43:207–216
- Ozawa T (1968) Chemical analysis of volcanic gases: I. Chemical analysis of volcanic gases containing water vapor, hydrogen chloride, sulfur dioxide, hydrogen sulfide, carbon dioxide, etc. *Geochem Int* 5:939–947
- Richet P, Bottinga Y, Javoy M (1977) A review of hydrogen, carbon, nitrogen, oxygen, sulphur, and chlorine stable isotope fractionation among gaseous molecules. *Ann Rev Earth Planet Sci* 5:65–110
- Taran YA, Giggenbach WF (2003) Geochemistry of light hydrocarbons in subduction-related volcanic and hydrothermal fluids. *Soc Econ Geol Special Publ* 10(2003):61–74
- Tsujihara R, Ishibashi H, Hokanishi N, Yasuda A (2017) Pre-eruptive process of the 60Ka caldera-forming eruption at Hakone volcano. In: Program and abstracts the volcanological Society of Japan, P005. https://doi.org/10.18940/vsj.2017.0_125 (in Japanese)
- Tsunogai U, Kamimura K, Anzai S, Nakagawa F, Komatsu D (2011) Hydrogen isotopes in volcanic plumes: tracers for remote temperature sensing of fumaroles. *Geochim Cosmochim Acta* 75:4531–4546
- Yukutake Y, Honda R, Harada M, Arai R, Matsubara M (2015) A magma-hydrothermal system beneath Hakone volcano, central Japan, revealed by highly resolved velocity structures. *J Geophys Res Solid Earth* 120:3293–3308. <https://doi.org/10.1002/2014JB011856>

Submit your manuscript to a SpringerOpen® journal and benefit from:

- Convenient online submission
- Rigorous peer review
- Open access: articles freely available online
- High visibility within the field
- Retaining the copyright to your article

Submit your next manuscript at ► springeropen.com